The science case and data processing strategy for the Thinned Aperture Light Collector (TALC): a project for a 20 m far-infrared space telescope

Marc Sauvage[a], Pierre Chanial[b], Gilles A. Durand[a], Louis R. Rodriguez[a], Jean-Luc Starck[a], Samuel Ronayette[a], Hervé Aussel[a], Vincent Minier[a], Frédérique Motte[a], Eric J. Pantin[a], Florent Sureau[c] and Robin Terrisse[d]

[a]Laboratoire AIM, CEA/Irfu, CNRS/INSU, Université Paris Diderot, CEA-Saclay, 91191 Gif-sur Yvette Cedex, France;
[b]APC, Astroparticule et Cosmologie, Université Paris Diderot, Bâtiment Condorcet, 10 rue Alice Domon et Léonie Duquet, 75205, Paris Cedex 13, France;
[c]CEA/DSM/Irfu/SEDI, C. E. Saclay, 91191 Gif sur Yvette Cedex, France;
[d]École Normale Supérieure de Lyon, 15 parvis René Descartes, BP 7000 69342 Lyon

ABSTRACT

The future of far-infrared observations rests on our capacity to reach sub-arcsecond angular resolution around 100 μm, in order to achieve a significant advance with respect to our current capabilities. Furthermore, by reaching this angular resolution we can bridge the gap between capacities offered by the JWST in the near infrared and those allowed by ALMA in the submillimeter, and thus benefit from similar resolving capacities over the whole wavelength range where interstellar dust radiates and where key atomic and molecular transitions are found.

In an accompanying paper,[1] we present a concept of a deployable annular telescope, named TALC for Thinned Aperture Light Collector, reaching 20 m in diameter. Being annular, this telescope features a main beam width equivalent to that of a 27 m telescope, i.e. an angular resolution of 0.92" at 100 μm. In this paper we focus on the science case of such a telescope as well on the aspects of unconventional data processing that come with this unconventional optical configuration.

The principal science cases of TALC revolve around its imaging capacities, that allow resolving the Kuiper belt in extra-solar planetary systems, or the filamentary scale in star forming clouds all the way to the Galactic Center, or the Narrow Line Region in Active Galactic Nuclei of the Local Group, or breaking the confusion limit to resolve the Cosmic Infrared Background. Equipping this telescope with detectors capable of imaging polarimetry offers as well the extremely interesting perspective to study the influence of the magnetic field in structuring the interstellar medium.

We will then present simulations of the optical performance of such a telescope. The main feature of an annular telescope is the small amount of energy contained in the main beam, around 30% for the studied configuration, and the presence of bright diffraction rings. Using simulated point spread functions for realistic broad-band filters, we study the observing performance of TALC in typical situations, i.e a field of point sources, and fields with emission power at every physical scales, taken to represent an extragalactic deep field observation and an interstellar medium observation. We investigate different inversion techniques to try and recover the information present in the input field. We show that techniques combining a forward modeling of the observation process and a reconstruction algorithm exploiting the concept of sparsity (i.e. related to the more general field of compressed sensing) represent a promising avenue to reach the angular resolution promised by the main beam of TALC.

Keywords: Far-infrared astronomy, space telescopes, deployable telescope, sparsity, signal processing, star formation, proto-planetary systems, Active Galactic Nuclei

Space Telescopes and Instrumentation 2014: Optical, Infrared, and Millimeter Wave, edited by Jacobus M. Oschmann, Jr., Mark Clampin, Giovanni G. Fazio, Howard A. MacEwen, Proc. of SPIE Vol. 9143, 91431B · © 2014 SPIE
CCC code: 0277-786X/14/$18 · doi: 10.1117/12.2055557

1. INTRODUCTION

The far-infrared (FIR) part of the electromagnetic spectrum (25-500 μm) contains around half of the post-big bang energy and nearly all of the photons that come to us from all astrophysical processes. Yet access to this waveband remains challenging for basic reasons: the atmosphere is largely opaque, telescopes must be large and cold, and detector technology has come of age only recently.

Science exploiting the FIR domain is thus relatively young, yet already demonstrates an impressive track record: a succession of facilities – *KAO*, *IRAS*, *COBE*, *ISO*, *Spitzer*, *AKARI*, *Planck* and *Herschel* – allowed us to gaze into the obscured Universe, advancing our understanding of cosmology, star and galaxy formation, and the origin of planetary systems. Despite these developments, FIR observational capabilities remain primitive in comparison with the optical/NIR region. FIR space facilities have been limited in aperture by the need for cryogenic cooling, which restricted the telescope size to <1 m for *IRAS*, *ISO*, *AKARI* and *Spitzer*. *Herschel* had the largest possible telescope, given technical and budget constraints, but this aperture could only be passively cooled, to $\sim$ 85 K, imposing a fundamental limit to the achievable sensitivity: in the early 21^{st} century, our most advanced facility, *Herschel*, delivered an angular resolution no better than Galileo's telescope and was operated against a blinding thermal background. Despite this, much of its success is attributable to the enhanced angular resolution provided by its 3.5-m aperture.

An additional reason for the productivity of this FIR facility is the vast areas of science that benefit from peering into this wavelength range. This is first due to the fact that thermal emission from dust associated with star formation peaks in the FIR, but more importantly to the presence of emission signatures that are both unique to this part of the spectral domain, and also unique in the access that they provide to the underlying physics. Via dust features in the continuum emission, we access the dust composition, size distribution and formation scenario, about which we know precious little; through ice features we can study critical evolutionary processes in the dense phases of the ISM; fine-structure lines found in the FIR give access to the thermal balance in the regions observed; for redshifted sources, we access the mid-IR range, where we find unambiguous diagnostics for the presence of active galactic nuclei; finally, the FIR offers a vast array of molecular tracers, among which the simple hydrides that represent a unique diagnostic for the build-up of molecular complexity, and water, whose transitions are key probes of the star-formation process and in assessing habitability for exo-planetary systems.

This being said, one must also realize that with the end of *Herschel*'s operations in April 2013, there are no more facilities in operation that allows access to the FIR. While this is clearly a problem for a number of science issues, the situation is no so bleak as it may seem. First, the *ALMA* observatory is close to reaching it full operational power, and while it is more adapted to the sub-millimeter range, its very high spectral and spatial resolutions allow addressing a number of science questions raised by *Herschel* (in particular regarding star formation processes). In the near future, the *JWST* and its mid-infrared instrument MIRI[2] will also be able to provide follow-up observations on *Herschel* science cases such as protoplanetary and debris disks. Both facilities will provide unprecedented spatial details, however none of them will be able to observe at the FIR peak, where emission traces most of the mass in the sources.

Two significant steps toward improving our access to the FIR domain are in the plans for the next two decades. Closer to us, the *CCAT* telescope[3] will deliver in 2019 diffraction-limited images at 350 μm from a 25 m telescope located at an altitude of 5600 m (i.e. a spatial resolution slightly better than *Herschel* in its shortest wavebands). With essentially a dry atmosphere above it, CCAT will be able to peer down to 200 μm for a fraction of its observing time, thus brushing the long-wavelength part of the FIR peak. In the more distant and therefore uncertain future lies the *SPICA*[4] project, a JAXA-led space telescope. With it cooled mirror, it promises to be limited only by natural backgrounds (e.g. zodiacal light), however with a mirror diameter about the same size as *Herschel*'s, a strong limiting factor will be source confusion.

Thus it is quite clear that no project currently planned will allow to observe the main part of the FIR peak (i.e. 50-200 μm) with a spatial resolution comparable to that delivered by operating, or planned facilities in neighboring wavelength ranges. This "FIR gap" is a high risk for the progress of science issues related to the cold Universe, and is the one we address with the TALC project.

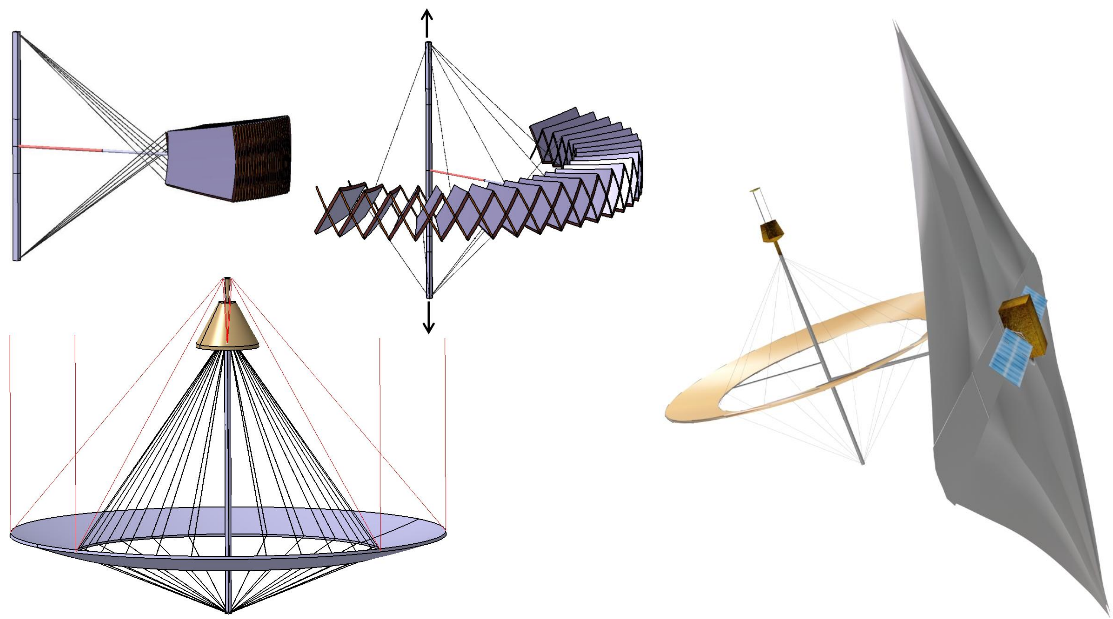

Figure 1. *left:* a sketch of TALC's primary mirror in different phases of its deployment. Clockwise from top left: the stack of mirror segments is pushed away from the central mast by a perpendicular extensible mast, then the central mast extends, causing the stack of mirrors to rotate and deploy, to finally close in deployed annular shape. In the last element of the figure, the module located on the top of the central mast supports the secondary mirror and contains the focal plane instrument(s). The light path is indicated to show that it never crosses the cable structure that holds the mirrors together. *Right:* a computer rendition of the complete spacecraft, with the annular telescope shielded behind a sunscreen, and a service module on the exposed side of the sunscreen.

2. TALC'S MAIN SCIENCE CAPACITIES

The principles of the TALC telescope (for Thinned Aperture Light Collector) are presented in detailed in an accompanying paper[1] but we briefly recall them here for clarity. TALC is built as a response to the question: "how can we send a single-dish telescope in space while going around the fact that the fairing's dimensions are the ultimate constraint to the telescope diameter?". For monolithic mirrors, such as *Herschel* or *SPICA*, the telescope diameter is limited by the fairing's diameter to 3-4 m. For segmented mirrors, such as the *JWST*, the fairing's length is the limit to the telescope diameter. TALC circumvents this by getting rid of the central part of the single dish, and using a fan-like system to deploy a stack of 24 mirrors into a ring telescope, 20 m in outer diameter (see Figure 1).

The main characteristics of TALC that can be recalled in the context of this paper are the following:

- At 20 m diameter, and with a ring width of 3 m, TALC has an exceptional collecting surface. In fact, it has the same collecting surface as the hole in its center, or approximately 16 times that of *Herschel*. Furthermore, because we have removed the central part of the telescope, the full width at half maximum (FWHM) of the main beam is equivalent to that of a single dish telescope of 27 m diameter, albeit with significantly larger side-lobes than a single dish. At 100 μm this is 0.9", 8 times better than *Herschel* at the same wavelength, and similar to *CCAT*. Therefore, provided the data processing is able to cope with the PSF side lobes, TALC can bring much progress toward closing the "FIR gap" both in angular resolution and sensitivity.
- TALC's optical design is such that it gives access to a relatively large instantaneous field of view of $2'$ radius undistorted. While very far from the degree-size field of view of *CCAT*, this is already significant, either to share the focal plane between instruments (see below) or to map it with large area detectors. This makes TALC a telescope concept oriented toward survey or large-area science, rather than high-resolution small-field science, to complement nicely the possibilities offered by *ALMA*

- We foresee to place the telescope behind a sunshield (right-hand panel of Figure 1), in a configuration similar to the *JWST*'s. This would allow it to access great circles on the sky going over the ecliptic poles, thus maximizing sky accessibility (i.e. the field of regard) contrary to interferometric concepts that are often restricted to point in the ecliptic plane.
- Although the instrument bay appears small on Figure 1, one has to remember the actual scale of the figure, where the diameter of the annulus is 20 m. Thus the base of the bay is close to three meter in diameter. This implies that one or two relatively large instruments can be installed in the focal plane, to accommodate, for instance, imaging and spectroscopic facilities.

While we mention above the possibility of fitting TALC with a suite of instruments, we are currently envisioning its science cases and the associated data processing research in the context of an imaging or survey telescope, with access to medium resolution spectroscopy (e.g. typically an integral field unit instrument), in order to take advantage of its high sensitivity, full (u, v) plane sampling, large instantaneous field-of-view (FoV) and all-sky access.

3. THE SCIENCE

3.1 Disks as birthplaces of planets

Exoplanets are uncovered almost daily now. Furthermore, the large space agencies are planning missions[5] that will completely fill the parameter space for extra solar planets (mass, type, orbit), including earth analogues, by the end of the next decade. We will thus be in a situation where the diversity of planetary system, and the relevance of the Solar System in that context, will be known. However the situation will be much less so for the precursors of these planetary systems, i.e. the protoplanetary disks, leaving large uncertainties in our understanding of the initial conditions for planet formation. *SPICA*, thanks to its much increased sensitivity, will be able to perform medium resolution spectroscopic studies of many disks but it will unfortunately resolve only very few of these disks leaving much to be learned with respect to their structural properties. On the other hand, ALMA and the JWST will resolve many disks but will be unable to derive precise measurement of the dust and gas distribution and composition for lack of the adequate and/or direct tracer. Regarding the dust, it is only by mapping it at the peak of its emission that one can properly account for the effect of the temperature and thus derive a proper mass. It is also in the FIR that specific solid-state features can reveal the nature and processing history of dust, further lifting ambiguities on mass measurements. As for gaseous components, the water lines, which are essential to understand how water is delivered from the interstellar medium to the planets in the habitable zone, are only accessible in the FIR, and the same situation is true for the HD lines which has been shown by *Herschel* to be a promising gas tracer in disks.[6]

On the related matter of later evolution of planetary systems, TALC will be very powerful for the study of so-called debris disks. *Herschel*, and therefore *SPICA* as well, could only resolve a handful of objects, among them the so-called "big 4", β Pic, Fomalhaut, ϵ Eridani and AU Mic. With its much-improved resolving power, TALC brings the promises of giving access to a significantly larger sample of stars with circumstellar material. Taking the example of recent Herschel observations of debris disks,[7,8] the characteristic scale to resolve to allow modeling of the disk is ~100 AU. With TALC, this scale is resolved at 100 μm up to 110 pc. Browsing through the catalog of resolved circumstellar disks known so far (maintained at *circumstellardisk.org*), we see that out of the 163 disks known today, 41 are located within 110 pc, and 3/4 of them have a disk whose diameter is larger than 100 AU (we also point that larger disks exist at larger distance hence these numbers are conservative estimates, even today). Thus there would be a significant increase in the number of disks accessible for detailed studies with TALC.

3.2 The initial mass function at the high mass end and in external galaxies

High-mass stars, while much less numerous than their lower mass counterpart and providing a negligible fraction of the total stellar mass in galaxies, are yet one of their fundamental constituent through their impact on the observable spectral energy distribution of galaxies or through the feedback processes they generate in the ISM (ionization, photo-dissociation, shocks, and metal enrichment). Yet little is know of their formation process both inside and outside of our Galaxy. This is essentially because they are rare and unfortunately distant, so that *Herschel*-like resolution cannot distinguish bona-fide massive proto-stars from proto-clusters. High angular resolution is required here,[9] but it has to be associated with the capacity to map large areas to (1) build statistically meaningful samples, and (2) connect the population of massive proto-stars to the cloud properties. Only with these two elements can we build a solid scenario for their formation. While *ALMA* is unbeatable to peer through massive condensations to see whether they are already fragmented, TALC would provide the ability to perform complete survey of high-mass star forming regions with high spatial scale fidelity from the large cloud scale down to those necessary to separate fragmented proto-clusters from massive proto-stars.

An interesting instrumental capacity for TALC would be to equip it to measure the FIR continuum polarization. This would give access to the strength and orientation of the magnetic field in the dense and warm regions of the ISM (complementing *ALMA* that will measure this polarization in the diffuse and cold regions). This offers the prospect of understanding how the magnetic field participates in the generation of structures in the ISM and ultimately in the star formation process. This is a rather unique niche for a telescope such as TALC and a field where very little is known even if the magnetic field is known to store a significant fraction of the energy at large scales in the ISM. While quite a number of teams are embarking on experiments that will measure polarization in the FIR and sub-millimeter regime, the angular resolution that these plan to reach will not provide answers regarding the structure of the interstellar medium given that the scales to resolve are typically around 0.1 pc.[10] Thus a combination of *ALMA* and TALC polarization studies of the ISM structure is bound to reveal much regarding the precursor conditions to star formation throughout our Galaxy and even reaching the Large Magellanic Cloud.

3.3 Disentangling AGN and star formation in galaxy evolution

Galaxy evolution is the result of three main processes: star formation, proceeding either through bursts following the merging of two galaxies or in a more secular way, accretion of matter onto black-holes in Active Galactic Nuclei, and the feedback processes associated to both phenomena. These processes jointly determine the energy budget of a galaxy throughout its evolution and an evolutionary sequence from starburst-dominated through active nuclei has been suggested.[11,12] The growth of bulges through star formation may be directly linked to the growth of black holes through accretion, resulting in the tight local correlation between the mass of the stellar spheroid and the central black hole.[13]

Much of this evolution is hidden by dust, causing up to hundreds of magnitudes of optical extinction. Uniquely, rest-frame mid-infrared (MIR) to FIR spectroscopy is able to trace these physical processes. The heavily obscured ISM is energized by the host's star formation and its growing AGN, and IR spectroscopy provides the diagnostics to distinguish between and quantify the two, measuring the separate luminosity functions of accretion and star formation as a function of cosmic time. The FIR waveband offers a unique tool to study the effect of both radiative and dynamical feedback: high-resolution imaging spectroscopy ($< 1"$, $R \sim 1000$) at rest-frame 20–60 μm (observed FIR) allows us to distinguish between the AGN-heated and starburst-heated components and constrain the possible joint evolutionary scenarios for galaxies and QSOs.[14] Imaging spectroscopy in the FIR waveband is thus the most important observational tool required to measure star formation as a function of redshift, whilst disentangling the effects of black-hole accretion, thereby elucidating what we know of galaxy/QSO evolution during the period when galaxies and AGN undergo their most significant evolution. FIR observations are absolutely key here, as they allow to follow key tracers (MIR continuum, MIR and FIR fine structure lines) over a period of time extending to a redshift of $\sim$3, i.e. the most important period in galaxy evolution. It is only for more distant objects that an observatory such as *ALMA* becomes essential.

4. DATA PROCESSING STRATEGIES

The science cases discussed above rely on the assumption that we can reach the full imaging power promised by a telescope such as TALC. In other terms they assume that we can benefit from the full resolving power of the telescope, and that the image fidelity is at its maximum. These two facts are not granted in the configuration of an annular telescope. As mentioned above, the benefit of having a sharper FWHM comes at the cost of having less energy in the central beam of the point spread function (PSF). Thus one has to study carefully the resulting resolving power as the effect of source confusion can a priori be more severe than with a filled single-dish

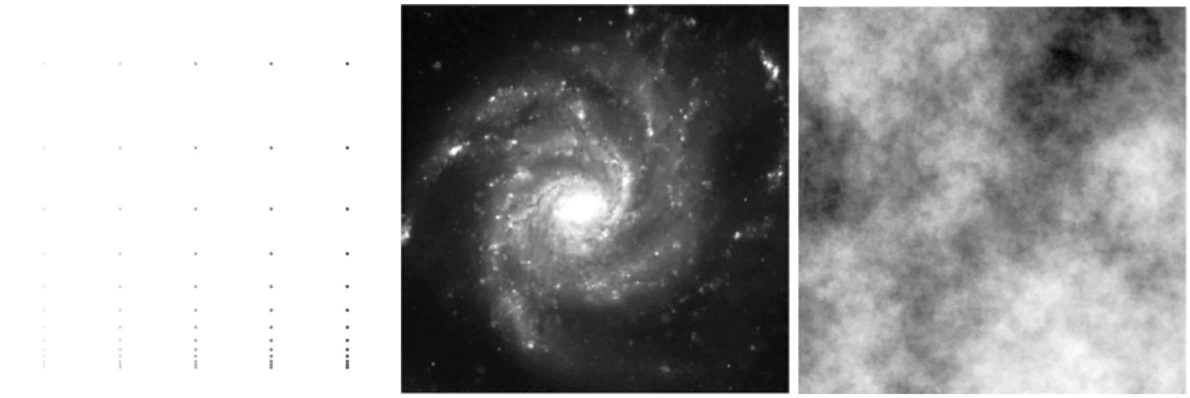

Figure 2. The typical astronomical scenes used to study possible data processing strategies that would allow reaching the full observing power of TALC. From left to right: a field of point sources, with sources placed increasingly closer to each other, and for a series of intensities. For the figure we have smoothed the scene so that sources become visible (otherwise they only cover a single pixel) and reveal the 5 different level of intensities, and the 13 source positions. A grand-design spiral galaxy, M101 observed in the optical, to provide spatial details before convolution with the TALC PSF. An ISM field with emission at every spatial scales generated by pink noise in the spatial domain.

telescope. Furthermore the particular beam shape of TALC realizes a complex convolution with the source plane and thus the image fidelity can be affected. We have therefore embarked in a series of simulations to explore the effect of TALC's beam on typical astronomical "scenes", to study possible data processing scenarios and their potential in restoring the full observational capacities of TALC.

These typical scenes are (1) a field of point sources placed on a grid with decreasing separation, exploring as well a range of source intensities, (2) an isolated grand-design galaxy, and (3) a "ISM" field with emission structure at every spatial scale. These typical scenes are presented on Figure 2.

4.1 The key problem: the point spread function

As mentioned before, the advantage of TALC with respect to a filled telescope of similar diameter is that the main beam is significantly thinner. In short this can be viewed as a consequence of the fact that we have removed the "smaller telescope" that formed the inner part of the filled structure, which would have contributed a larger main beam component. However in return this leads to the drawback that more energy is distributed outside of the main beam than in a filled telescope, with a higher contrast between bright and dark rings. As the angular location of these bright and dark rings is strongly wavelength-dependent, it can be more advantageous to implement narrow filters on TALC rather than wide ones. Nevertheless we have studied the full-system performance issues with a filter typical of what is used today, i.e. a central wavelength of 100 μm and a spectral resolution R of 5.

We have performed *Zemax* computations of the PSF for TALC and a filled telescope of identical collecting surface and compare, on Figure 3, the PSF and encircled energy fraction (EEF) of these two telescopes as well as that of the actual *Herschel*+PACS system. It is clear that TALC offers a significant improvement in resolution with respect to a *Herschel*-class telescope (e.g. *SPICA*): the first dark ring of TALC occurs at $\sim 1''$ while for a 3.5 m-class telescope it is at $7''$, TALC is also better than a filled telescope of equivalent surface where the first dark ring occurs around $2''$. However the figure also reveals the more complex PSF of TALC: the bright ring around the central peak reaches $1/10^{th}$ of the peak brightness while for a filled telescope it only reaches $1/100^{th}$ of the peak. The right-hand panel of Figure 3 reveals how this translates on the EEF: the EEF curves has its first flat portion (indicating the location of the main beam) when only 30% of the energy of the PSF is accounted for. In the filled mirror case this first plateau occurs when more than 80% of the PSF energy is accounted for. These features indicate that to extract the full benefit of the sharp main beam of TALC we will need to implement clever image reconstruction techniques.

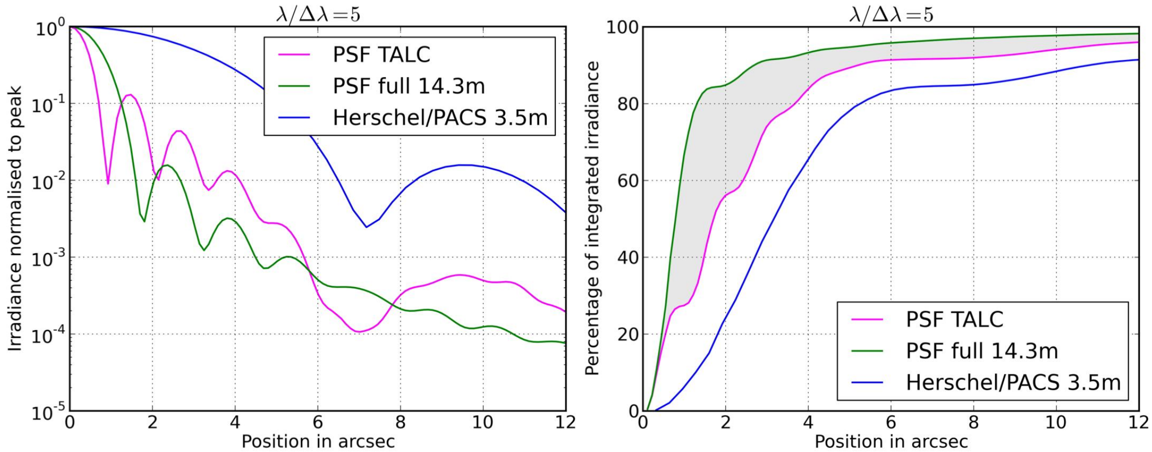

Figure 3. The optical Point Spread Function of TALC compared to reference architectures. The full telescope with 14.3 m diameter has the same collecting surface as TALC but in a classical single-dish configuration. *Herschel*/PACS is the effective PSF of the telescope+instrument as measured in space. The left panel shows the normalized profile of the PSF where we readily identify the gain in main beam width, but also the more complex situation presented by the ring structure around the main beam (when printed in b/w, the TALC PSF is the narrowest one and the *Herschel*/PACS one the widest). The right-hand panel shows the encircled energy fraction, which shows, as expected, that while TALC with its odd PSF is still significantly better than Herschel, a large fraction, about 70%, of the energy is outside the main beam (when printed in b/w the TALC EEF is the curve located below the grey shaded area, the curve located above it is the 14.3 m single-dish EEF. The *Herschel*/PACS EEF is the slowest growing curve).

4.2 Statement of the problem

Classical operations of an imaging or survey telescope consist in first recording the signal on the sky with a pointing pattern that tries to optimize the signal recording process against a number of issues (e.g. using cross-scanning or spiral patterns to try and beat the effect on $1/f$ noise when reconstructing the sky image) and then implement some back-projection* algorithm to build a map of the observed sky. Drizzling techniques[15] are typical examples of this back-projection process. While computationally performant this approach has a number of drawbacks. First, since the back-projection is not the exact inverse operation of the projection, it realizes an extra convolution of the data when building the map. Second, while the PSF effects are present at the projection stage (from sky to detector) it is very complex to deal with the PSF in the back-projection algorithm. Thus in such schemes, the treatment of PSF-induced artefacts is performed through deconvolution techniques that have their intrinsic limitations. More generally, map-making techniques that only concentrate on the back-projection stage generally do not describe, or even neglect, the processes that lead to signal being recorded by the pixels. Yet it is only when these processes are fully taken into account that optimal signal reconstruction can be reached.

This is what we have done in the present study: rather than trying to deconvolve a reconstructed image of the sky, we fully model the transfer of astronomical signal through the acquisition chain, integrating in the model all our knowledge of the process (e.g. pointing history, the particulars of the on-board acquisition scheme, noise properties when known...), and then invert this model. This concept of coupling the instrument design and properties with the algorithm performing the image reconstruction has been proposed in the Compressed Sensing theory[16] and already has had a wide impact in astrophysics, as a bibliographic research on the terms "compressed sensing" can reveal. A key element of this approach is to realize a fundamental feature of the astrophysical signal we want to reconstruct, namely its sparsity: for all the signals we want to reconstruct, there exists a base of orthogonal "vectors" (think for instance wavelets) where the signal can accurately be represented using a finite list of coefficients. In that case, the complex inversion problem of going back from the recorded

*We use the convention that the process that goes from the sky signal to the recorded signal is called a *projection* of the sky into the detector space, and the reverse process, i.e. using the recorded signal to build a map of the sky is called a *back-projection*.

signal to the original one is tractable even with a relatively small number of measurements (this has been applied, for instance, to reconstruct maps obtained by *Herschel*[17]). As the sparsity is in the original sky signal, and not in the data stream that is produced by the instrument, we need to have an accurate representation of the relation between the sky signal and the recorded data in order to exploit this property in the reconstruction of the sky signal.

4.3 Forward modeling of the acquisition process

To fully exploit the sparsity in the sky signal we want to reconstruct, i.e. to be able to formulate our data processing problem in the form $y = H \times x + n$, where x is the sky vector, y the recorded signal, and n the noise vector, we need to build the operator H that realizes the transfer from sky to signal space. H is an operator in the matrix sense, but in a more physical sense, it represents an instrument simulator. We capture in H all the operations that the observation of the sky realizes. Therefore H is the product of different matrices corresponding to (1) the pointing history of the observations, (2) the convolution produced by the telescope and instrument PSF, (3) detector effects, such as for instance a time constant in the response that can be expressed as a time convolution, (4) compression operations that are often present on-board when data transfer is limited...

The interest of this forward modeling approach is multiple. First it obviously requires that a clear understanding of the acquisition process is available, which is always positive. Then it provides a clear separation for all the different instrumental effects, such that their impact on the reconstructed sky can be studied, and either the observation strategy or the reconstruction algorithm can be optimized accordingly. Finally, it provides an efficient and modular way to realize an instrument simulator. A further advantage of this modular forward modeling approach is that the operator modules can be improved at will to provide an increasingly accurate representation of the observation. Futhermore, in the Compressed Sensing approach, the inversion strategy exploits sparsity constraints expressed on the solution of the inversion problem (x) such that optimization of the inversion algorithm can proceeds independently of the complexification of the transform operator H.

4.4 Results

In all the cases that we have simulated so far, the observation is performed in scanning mode, with the pointing history realizing two series of sweeps through the scene oriented at 90° from one another. In all cases, the scenes are observed with an $R = 5$ filter centered at $100\,\mu$m. In the present simulations, we have used only white noise, i.e. we have not considered the presence of $1/f$ noise.

To compare our results to those that would be obtained with a traditional approach, we have systematically built what we call the "naive" maps, where the map x is approximated by:

$$\hat{x} = \frac{H^{\mathrm{T}} y}{H^{\mathrm{T}} 1}, \tag{1}$$

where the upper term is the purely geometric back-projection of the recorded signal, and the lower term represents the coverage map to re-normalize the back-projection so that it is flux-conserving. It is clear that $\hat{x}$ is not an exact solution of our problem since $H^{\mathrm{T}} \neq H^{-1}$.

4.4.1 Point sources

In this test, we observe the point source network of Figure 2. The brightness of the sources changes from left to right in the proportion 1:100, with the separation decreasing from $15''$ to $0.5''$. To simulate the point sources, we take an input image with a pixel size of $0.11''$, and place all the flux in one pixel. The sources are assumed to have a constant spectral flux density ($f_\nu = cte$). We have added noise to a level representative of TALC (i.e. assuming its surface would be at 80 K, while the brightest source is at 100 mJy). As the scene to reconstruct is rather simple in that case, we have performed tests with a single method, the so-called direct one, where the objective function to minimize is:

$$J(x) = \|Hx - y\|^2_{2,N} + \lambda \|x\|_1 + \iota_C(x), \tag{2}$$

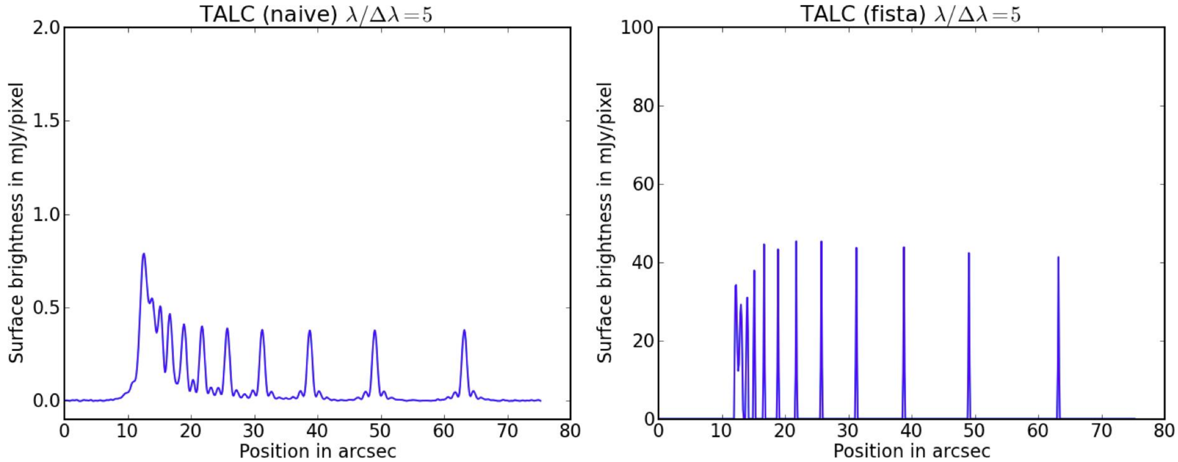

Figure 4. Spatial resolution restoration performance for (left) the "naive" approach, and (right) a full-inversion of the acquisition model exploiting the sparsity of the signal. The blue line is a 1-pixel-wide cut on the column containing the brightest pixel of the simulated sources. In the reconstructed images we use the same pixel size as the input image ($0.11''$).

where the first term expresses the likelihood of the sky given the data, the second one the sparsity of the sky, and the third one a positivity constraint on the sky. Resolving this equation is done with an implementation of the accelerated FISTA algorithm.[18]

Figure 4, left panel, shows a 1-pixel wide column cut of the reconstructed sky using the "naive" method. It clearly reveals the ringed structure of the PSF and shows the piling of neighboring sources at small separation: starting from the largest separation (right-hand side of the panel), only the first four sources are separated enough to allow accurate photometry. From the 5^{th} source onward, piling increases and already at the 6^{th} source we have reached confusion (i.e. the "background" flux is from the sources themselves). Much of the flux is also distributed outside of the central pixel, as expected, as is revealed by the peak intensity of only 0.5, when it was originally 100. The right-hand panel of Figure 4 shows a similar cut this time on a sky reconstructed by inverting a complete acquisition model of the observation and exploiting the sparsity of the sky signal (equation [2]). We are now able to restore a significant fraction of the total flux in the central pixel, and due to this the resolving power is very much increased as we see that source piling does not happen until we reach the 9^{th} source in the column. This is clearly a simulation of an ideal situation but it shows that innovative data processing will allow circumventing the limitations apparently imposed by the odd PSF of TALC. We have also tested the performance of the inversion method on the S/N ratio in the image and show that it preserves the relation between S/N and input source brightness as efficiently as the "naive" method.

4.4.2 Extended sources

As with the point source simulations, we simulate an observation consisting of two orthogonal scanning patterns, each of three legs with minimal overlaps to have the most homogenous coverage. Noise is added to the signal at the level expected for the thermal emission of an 80 K TALC mirror. We produced two images per type of field, one at low signal-to-noise ratio (SNR) where we typically have 0.2 mJy/pixel and one at high SNR where we typically have 2 mJy/pixel. We will characterize the accuracy of our reconstruction with an examination of the spatial power spectrum of the map, which provides a quick way to see how we have treated the imprint of the PSF on the observation[†].

The problem of an extended source requires (1) the choice of an adequate wavelet family to decompose the sky image (compared to the simpler choice of working on the image itself as in the case of point sources), (2) the definition of an "objective" function (or "cost" function) that quantifies the difference between the sky and its

[†]Incidentally, in some science cases, the power spectrum of the observed structure is the information of choice, which, in the context of compressed sensing, would allow for a different data processing strategy where we skip the map reconstruction x to work directly on the power spectrum.

reconstruction and has to be minimized, and (3) the identification of the algorithm that will actually minimize that function. For this preliminary study, we have only considered Haar and Daubechies wavelet transforms. An interesting exploration will be the à-trou wavelet transform, whose redundancy allows the translation-invariance of the elements of the wavelet dictionary.

Among the many objective functions of potential interest, we will consider the minimization of the following three:

$$\begin{aligned} J(x) &= \|Hx - y\|^2_{2,N} + \lambda \|x\|_1 + \iota_C(x), \\ J(x) &= \|Hx - y\|^2_{2,N} + \lambda \|W^T x\|_1 + \iota_C(x), \\ J(x) &= \|Hx - y\|^2_{2,N} + \lambda \|\omega\|_1 + \iota_C(W\omega), \end{aligned} \tag{3}$$

x denotes the image in the direct space, and ω the image in the wavelet space. W is the wavelet-to-direct transform, N the time-time noise correlation matrix and ι_C the indicator over the convex set $C = \{(x_i) \in \mathbb{R}_n \mid \forall i, x_i \geq 0\}$. The first term is the data fidelity term (here, the likelihood), the second one adds a sparsity constraint (in the direct or wavelet space) and the third one a positivity constraint. In Equation [3] the first line corresponds the direct problem that we have used to study the point source reconstruction, the second line is often called the analysis problem and the third, the synthesis problem. For the first case, the accelerated FISTA algorithm is an appropriate choice while for the other two, the first-order primal-dual algorithm[19] and the generalized forward-backward algorithm (GFB[20]) are preferred respectively. Although the analysis formulation is thought to give a sky estimate less affected by ringing effects in regions of strong gradients, the Chambolle-Pock algorithm[19] is not accelerated and thus for time-constraints reason, we have started our study by using the FISTA and GFB algorithms. We stress that optimization of algorithms solving Equations [3] is a very active field of research and that significant theoretical advances in convergence acceleration are very likely in coming years.

Figure 5 presents the results of our investigations for the two extended source simulations. We show two series of 3×2 images, for the cirrus field on the left and for the galaxy field on the right. The cirrus field tests our ability to restore the power spectrum on a statistical basis, while the galaxy field combines extended structure with point sources. Top-left of each series shows the original image, while the top-right image is as reconstructed with the "naive" method. The middle series show the result of the synthesis problem (third line in Equations [3]), for high and low SNR, while the bottom series shows the result of direct problem (first line in Equations [3]). Visually speaking the reconstructed maps are already quite satisfying. They show a drastic improvement over the naive reconstruction where many details had been lost. However we clearly see that there is room for improvement:

- The low-SNR maps show a ringing pattern all over the image, which is clearly unacceptable given that we expect to be reaching this kind of surface brightness level. We do see however that working in wavelet space (GFB) rather than in the image space (FISTA) already brings some improvement to this effect, which is encouraging.
- The ringing around bright point sources is not properly corrected at high flux level (this is visible in the group of images corresponding to the galaxy simulation).

We can also compare these results in a more quantitative way by inspecting the spatial power spectra of the images, which we show in the following figures. In these figures we plot the ratio of the power spectrum of the reconstructed image as a function of the power spectrum of the original image as a function of the angular frequency (i.e. the inverse of the scale-length, so that the large scales are on the left side of the graphs), for the cirrus field on the left and the galaxy field on the right.

The blue curves correspond to the naively reconstructed image. They show how the small main beam efficiency of TALC combined with a method that ignores it conspire to significantly affect the structures in the map (even large scales are affected due to the fact that the TALC PSF distributes energy far away from its center). At scales smaller than the main beam, essentially all information is lost. The red curves show the result of the FISTA reconstruction, with the dotted curves corresponding to the low SNR images. For the high SNR

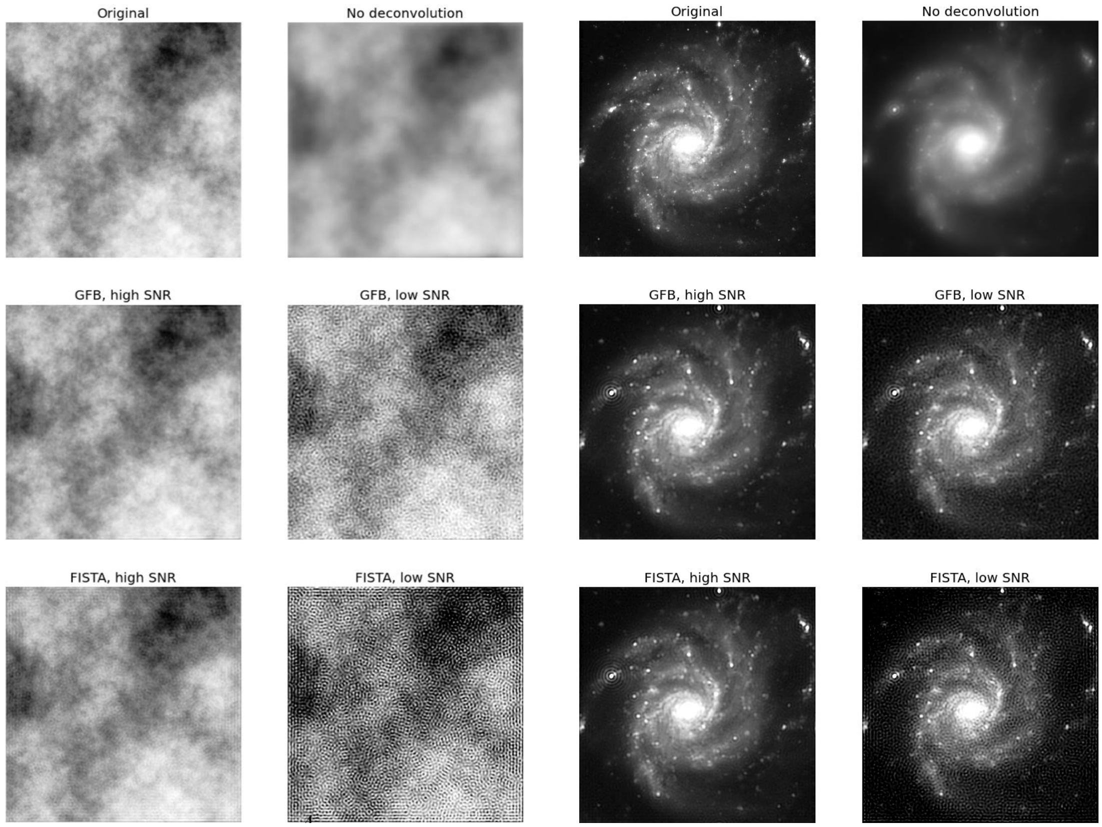

Figure 5. Results of our reconstruction methods for the two extended fields, the cirrus field on the left and the spiral galaxy on the right. For each field the top left panel is the original image and the top right panel is the image reconstructed with the "naive" method. The next two lines show the performance of the two algorithmic approaches used here, for two different SNR levels.

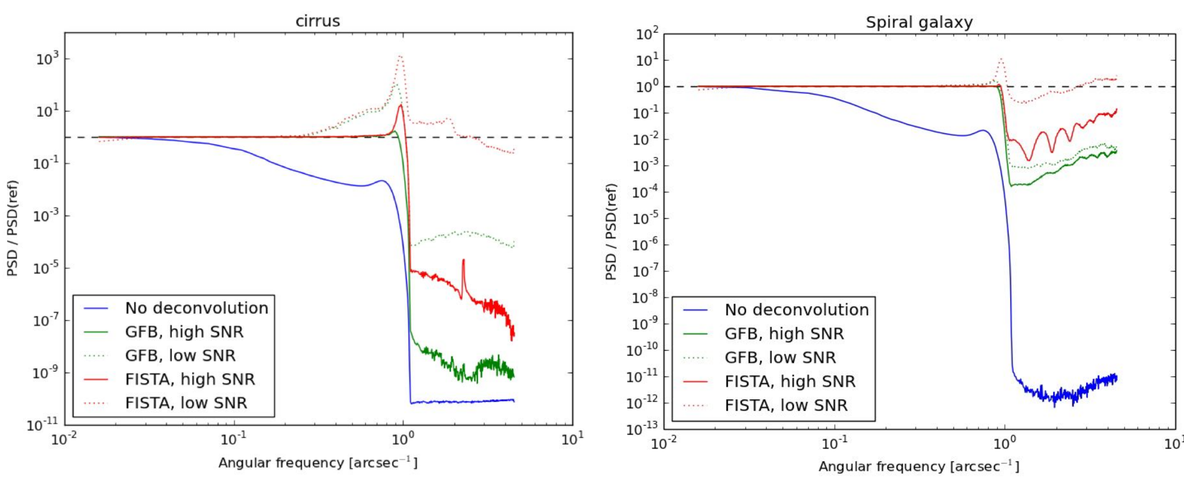

Figure 6. The ratio of the spatial power spectrum in the reconstructed image over that of the original image, for the different reconstruction methods experimented with in this paper. The left-hand panel corresponds to the Cirrus field simulation, and the right-hand panel to the spiral galaxy simulation. In b/w prints, the curves are arranged in the following way: concentrating on the part of the figures below scales of $1''$ (right-hand part of the panels), from bottom to top, one finds, in continuous lines, the "naive" PSD ratio, the GFB ratio, and the FISTA ratio. Low SNR curves are the dotted ones, and follow the same order as the high SNR ones.

images the situation is quite significantly improved with the PSD ratio staying close to 1 almost down to the main beam scale. The situation is not yet ideal as we see an overshoot when we approach the main beam scale. For the low SNR the situation is worse as we see an increase of the PSD ratio, corresponding to the ringing structure we see all over the images. The GFB method appears again better suited than the FISTA method to deal with scales approaching the main beam scale, as the green curves show. The overshooting in the PFD ratio (creation of structures that were not in the original map) is of also of smaller amplitude than what it is with FISTA. In any case, these reconstruction methods show that they are promising avenues to circumvent the dramatic impact that TALC's peculiar PSF has on the structures present in the map.

5. CONCLUSIONS AND FUTURE PROSPECTS

We believe that the analysis we have presented here shows that an annular telescope such as TALC[1] can deliver on extremely interesting science cases related to FIR imaging and spectro-imaging, provided appropriate data processing methods are developed. Following developments occurring around the concepts of compressed sensing and sparsity, we show here that the prospect of dealing adequately with the adverse effects of a highly structured, and "dispersed" point spread function is fully in reach. We are also quite aware that the analysis presented here is still in its early phases and intend to concentrate in the future on aspects that will render it both more robust and more realistic with respect to the expected artefacts a telescope such as TALC creates. These aspects will include:

- Exploring more wavelet bases and in particular redundant ones (e.g. the à-trou wavelet base).
- Fully investigating the analysis problem (second line of Equations [3]).
- Dealing with the bright point source artifact (which could require a change of the objective function).
- Implementing non-perfect PSF in the transform operator H (such as resulting from an improperly phased telescope, as well as from the segmented nature of the telescope).

ACKNOWLEDGMENTS

This work was granted access to HPC resources at the French National Computing Center Curie under grant no. 2013046661 funded by the GENCI (Grand Equipement National de Calcul Intensif). The software tools developed by one of us (P. Chanial) are part of a python package `PySimulators` freely available at `http://pchanial.github.io/pysimulators`.

REFERENCES

[1] G. A. Durand, M. Sauvage, L. R. Rodriguez, S. Ronayette, P. Chanial, Scolam L., A. Bonnet, V. Revéret, H. Aussel, M. Carty, V. Minier, P. Tremblin, E. Pantin, M. Berthé, J. Martignac, F. Motte, M. Talvard, T. Tourette, J.-L. Starck, D. L., and D. M., "A new deployable concept for a 20-m far-infrared space telescope," in *This Conference*, *Society of Photo-Optical Instrumentation Engineers (SPIE) Conference Series*, 2014.

[2] G. S. Wright, G. H. Rieke, L. Colina, E. van Dishoeck, G. Goodson, T. Greene, P.-O. Lagage, A. Karnik, S. D. Lambros, D. Lemke, M. Meixner, H.-U. Norgaard, G. Oloffson, T. Ray, M. Ressler, C. Waelkens, D. Wright, and A. Zhender, "The JWST MIRI instrument concept," in *Optical, Infrared, and Millimeter Space Telescopes*, J. C. Mather, ed., *Society of Photo-Optical Instrumentation Engineers (SPIE) Conference Series* **5487**, pp. 653–663, Oct. 2004.

[3] D. Woody, S. Padin, E. Chauvin, B. Clavel, G. Cortes, A. Kissil, J. Lou, P. Rasmussen, D. Redding, and J. Zolwoker, "The CCAT 25m diameter submillimeter-wave telescope," in *Society of Photo-Optical Instrumentation Engineers (SPIE) Conference Series*, *Society of Photo-Optical Instrumentation Engineers (SPIE) Conference Series* **8444**, Sept. 2012.

[4] T. Nakagawa, H. Matsuhara, and Y. Kawakatsu, "The next-generation infrared space telescope SPICA," in *Society of Photo-Optical Instrumentation Engineers (SPIE) Conference Series*, *Society of Photo-Optical Instrumentation Engineers (SPIE) Conference Series* **8442**, Sept. 2012.

[5] H. Rauer, C. Catala, C. Aerts, T. Appourchaux, W. Benz, A. Brandeker, J. Christensen-Dalsgaard, M. Deleuil, L. Gizon, M.-J. Goupil, M. Güdel, E. Janot-Pacheco, M. Mas-Hesse, I. Pagano, G. Piotto, D. Pollacco, N. C. Santos, A. Smith, J. -C., Suárez, R. Szabó, S. Udry, V. Adibekyan, Y. Alibert, J.-M. Almenara, P. Amaro-Seoane, M. Ammler-von Eiff, M. Asplund, E. Antonello, W. Ball, S. Barnes, F. Baudin, K. Belkacem, M. Bergemann, G. Bihain, A. C. Birch, X. Bonfils, I. Boisse, A. S. Bonomo, F. Borsa, I. M. Brandão, E. Brocato, S. Brun, M. Burleigh, R. Burston, J. Cabrera, S. Cassisi, W. Chaplin, S. Charpinet, C. Chiappini, R. P. Church, S. Csizmadia, M. Cunha, M. Damasso, M. B. Davies, H. J. Deeg, R. F. Díaz, S. Dreizler, C. Dreyer, P. Eggenberger, D. Ehrenreich, P. Eigmüller, A. Erikson, R. Farmer, S. Feltzing, F. de Oliveira Fialho, P. Figueira, T. Forveille, M. Fridlund, R. A. García, P. Giommi, G. Giuffrida, M. Godolt, J. Gomes da Silva, T. Granzer, J. L. Grenfell, A. Grotsch-Noels, E. Günther, C. A. Haswell, A. P. Hatzes, G. Hébrard, S. Hekker, R. Helled, K. Heng, J. M. Jenkins, A. Johansen, M. L. Khodachenko, K. G. Kislyakova, W. Kley, U. Kolb, N. Krivova, F. Kupka, H. Lammer, A. F. Lanza, Y. Lebreton, D. Magrin, P. Marcos-Arenal, P. M. Marrese, J. P. Marques, J. Martins, S. Mathis, S. Mathur, S. Messina, A. Miglio, J. Montalban, M. Montalto, M. J. P. F. G. Monteiro, H. Moradi, E. Moravveji, C. Mordasini, T. Morel, A. Mortier, V. Nascimbeni, R. P. Nelson, M. B. Nielsen, L. Noack, A. J. Norton, A. Ofir, M. Oshagh, R.-M. Ouazzani, P. Pápics, V. C. Parro, P. Petit, B. Plez, E. Poretti, A. Quirrenbach, R. Ragazzoni, G. Raimondo, M. Rainer, D. R. Reese, R. Redmer, S. Reffert, B. Rojas-Ayala, I. W. Roxburgh, S. Salmon, A. Santerne, J. Schneider, J. Schou, S. Schuh, H. Schunker, A. Silva-Valio, R. Silvotti, I. Skillen, I. Snellen, F. Sohl, S. G. Sousa, A. Sozzetti, D. Stello, K. G. Strassmeier, M. Švanda, G. M. Szabó, A. Tkachenko, D. Valencia, V. van Grootel, S. D. Vauclair, P. Ventura, F. W. Wagner, N. A. Walton, J. Weingrill, S. C. Werner, P. J. Wheatley, and K. Zwintz, "The PLATO 2.0 Mission," *ArXiv e-prints* , Oct. 2013.

[6] E. A. Bergin, L. I. Cleeves, U. Gorti, K. Zhang, G. A. Blake, J. D. Green, S. M. Andrews, N. J. Evans, II, T. Henning, K. Öberg, K. Pontoppidan, C. Qi, C. Salyk, and E. F. van Dishoeck, "An old disk still capable of forming a planetary system," *Nature* **493**, pp. 644–646, Jan. 2013.

[7] B. Acke, M. Min, C. Dominik, B. Vandenbussche, B. Sibthorpe, C. Waelkens, G. Olofsson, P. Degroote, K. Smolders, E. Pantin, M. J. Barlow, J. A. D. L. Blommaert, A. Brandeker, W. De Meester, W. R. F. Dent, K. Exter, J. Di Francesco, M. Fridlund, W. K. Gear, A. M. Glauser, J. S. Greaves, P. M. Harvey, T. Henning, M. R. Hogerheijde, W. S. Holland, R. Huygen, R. J. Ivison, C. Jean, R. Liseau, D. A. Naylor, G. L. Pilbratt, E. T. Polehampton, S. Regibo, P. Royer, A. Sicilia-Aguilar, and B. M. Swinyard, "Herschel images of Fomalhaut. An extrasolar Kuiper belt at the height of its dynamical activity," *A&A* **540**, p. A125, Apr. 2012.

[8] T. Löhne, J.-C. Augereau, S. Ertel, J. P. Marshall, C. Eiroa, A. Mora, O. Absil, K. Stapelfeldt, P. Thébault, A. Bayo, C. Del Burgo, W. Danchi, A. V. Krivov, J. Lebreton, G. Letawe, P. Magain, J. Maldonado, B. Montesinos, G. L. Pilbratt, G. J. White, and S. Wolf, "Modelling the huge, Herschel-resolved debris ring around HD 207129," *A&A* **537**, p. A110, Jan. 2012.

[9] S. Bontemps, F. Motte, T. Csengeri, and N. Schneider, "Fragmentation and mass segregation in the massive dense cores of Cygnus X," *A&A* **524**, p. A18, Dec. 2010.

[10] D. Arzoumanian, P. André, P. Didelon, V. Könyves, N. Schneider, A. Men'shchikov, T. Sousbie, A. Zavagno, S. Bontemps, J. di Francesco, M. Griffin, M. Hennemann, T. Hill, J. Kirk, P. Martin, V. Minier, S. Molinari, F. Motte, N. Peretto, S. Pezzuto, L. Spinoglio, D. Ward-Thompson, G. White, and C. D. Wilson, "Characterizing interstellar filaments with Herschel in IC 5146," *A&A* **529**, p. L6, May 2011.

[11] D. B. Sanders, B. T. Soifer, J. H. Elias, B. F. Madore, K. Matthews, G. Neugebauer, and N. Z. Scoville, "Ultraluminous infrared galaxies and the origin of quasars," *ApJ* **325**, pp. 74–91, Feb. 1988.

[12] T. Storchi-Bergmann, R. M. González Delgado, H. R. Schmitt, R. Cid Fernandes, and T. Heckman, "Circumnuclear Stellar Population, Morphology, and Environment of Seyfert 2 Galaxies: An Evolutionary Scenario," *ApJ* **559**, pp. 147–156, Sept. 2001.

[13] D. Merritt and L. Ferrarese, "The M-σ Relation for Supermassive Black Holes," *ApJ* **547**, pp. 140–145, Jan. 2001.

[14] D. Farrah, J. Bernard-Salas, H. W. W. Spoon, B. T. Soifer, L. Armus, B. Brandl, V. Charmandaris, V. Desai, S. Higdon, D. Devost, and J. Houck, "High-Resolution Mid-Infrared Spectroscopy of Ultraluminous Infrared Galaxies," *ApJ* **667**, pp. 149–169, Sept. 2007.

[15] A. S. Fruchter and R. N. Hook, "Drizzle: A Method for the Linear Reconstruction of Undersampled Images," *PASP* **114**, pp. 144–152, Feb. 2002.

[16] D. L. Donoho, "Compressed sensing," *IEEE Trans. Inform. Th.* **52**, pp. 1289–1306, 2006.

[17] N. Barbey, M. Sauvage, J.-L. Starck, R. Ottensamer, and P. Chanial, "Feasibility and performances of compressed sensing and sparse map-making with Herschel/PACS data," *A&A* **527**, p. A102, Mar. 2011.

[18] A. Beck and M. Teboulle, "Fast Gradient-Based Algorithms for Constrained Total Variation Image Denoising and Deblurring Problems," *IEEE Transactions on Image Processing* **18**, pp. 2419–2434, Nov. 2009.

[19] A. Chambolle and T. Pock, "A first-order primal-dual algorithm for convex problems withapplications to imaging," *Journal of Mathematical Imaging and Vision* **40**(1), pp. 120–145, 2011.

[20] H. Raguet, J. Fadili, and G. Peyré, "A generalized forward-backward splitting," *SIAM Journal on Imaging Sciences* **6**(3), pp. 1199–1226, 2013.